Grazing incidence X-ray absorption characterization of amorphous Zn-Sn-O thin film

S L Moffitt,[1] Q Ma,[2] D B Buchholz,[1] R P H Chang,[1] M J Bedzyk[1] and T O Mason[1]
[1]*Department of Materials Science and Engineering, Northwestern University, Evanston, Illinois 60208, USA*
[2]*DND-CAT, Northwestern Synchrotron Research Center at Advanced Photon Source, Argonne, Illinois 60439, USA*

E-mail: q-ma@northwestern.edu

Abstract. We report a surface structure study of an amorphous Zn-Sn-O (*a*-ZTO) transparent conducting film using the grazing incidence X-ray absorption spectroscopy technique. By setting the measuring angles far below the critical angle at which the total external reflection occurs, the details of the surface structure of a film or bulk can be successfully accessed. The results show that unlike in the film where Zn is severely under coordinated (N < 4), it is fully coordinated (N = 4) near the surface while the coordination number around Sn is slightly smaller near the surface than in the film. Despite a 30% Zn doping, the local structure in the film is rutile-like.

1. Introduction

Crystalline transparent conducting oxides (TCOs) have been widely used as transparent electrodes in flat panel displays, solar cells, light emitting diodes, etc [1]. There is, however, an increasing interest in amorphous (*a*-) TCOs in device applications. They have comparable electrical and optical properties to their crystalline counterparts [2]. In addition, amorphous films can be deposited at low temperature on flexible substrates, have good mechanical stabilities under stress [3] and smoother surface morphologies [4]. These are some of the prerequisites for flexible electronics.

Amorphous Zn-Sn-O (*a*-ZTO) films, besides being indium-free, have shown good electrical properties. A 10 at.% Zn-doped SnO_2 film, deposited by radio frequency (RF) magnetron sputtering, has shown conductivity of ~1000 S/cm after vacuum annealing at 300°C [5]. To understand the structural origin of their physical properties, X-ray absorption spectroscopy techniques are often used [2, 6]. However, surface structures are rarely addressed. Here, we report some preliminary results of grazing incidence X-ray absorption measurements on *a*-ZTO film with 30% Zn as an example.

2. Sample preparation and characterization

The *a*-ZTO thin film of 529 nm thick with 30 at.% Zn was deposited on 2×1 cm^2 fused quartz substrate at room temperature by a pulsed laser deposition (PLD) system employing a 248 nm KrF excimer laser. The laser beam was focused using a fused silica lens to a 1×2 mm^2 spot size on the targets, which were rotated at a rate of 5 rpm to prevent localized heating. A dual-target deposition method was employed, where the constituent oxides (ZnO and SnO_2) were used as the targets. The oxygen partial pressure was maintained at 18 mTorr. The film composition was controlled by the deposition time of each target and was later confirmed by energy dispersive X-ray analysis. The film thickness was measured by optical

ellipsometry. Carrier concentration (-7.2×10^{18} cm^{-3}), Hall mobility (10.2 $cm^2/V\cdot s$), and conductivity (12 S/cm) of the film were measured by Hall effect in van der Pauw configuration with a 0.58 Tesla field.

X-ray absorption measurements were carried out at the 5-BM-D beamline of the DND-CAT located at Sector 5 of the Advanced Photon Source (Argonne, IL). A Si(111) double-crystal monochromator was used for energy scan ($\Delta E/E = 1.4\times10^{-4}$). The incident X-ray intensity was 60% detuned for harmonic rejection and monitored by an ion chamber filled with gasses absorbing 10% of the incident X rays. The EXAFS data were all collected in fluorescence mode using 4-element Si-drifted solid state detectors (ME4). For the film EXAFS, the sample was held vertically with the X-ray incidence angle α=54˚ and the data were collected with a ME4 detector at 90˚ to the X-ray beam. For the surface EXAFS, the sample was placed on a two-circle Huber stage with its surface normal upward (or 90˚ to the synchrotron X-ray electric vector) and the data were collected with α < the critical angle θ_c using two ME4 detectors. The beam size was set using slits to 0.05×8 mm^2 for Zn K edge and to 0.02×8 mm^2 for Sn K edge. A second slit set was placed behind the sample for alignment. Direct and reflected beams were measured by an ion chamber with gasses absorbing 20% of the X rays. Figure 1 shows reflected and fluorescence intensities vs. θ measured 50 eV above Zn and Sn K edges, respectively. For energy scan to 600 eV above E_0, Changes in θ_c are negligibly small (<0.003˚ for Sn K edge and <0.01˚ for Zn K edge).

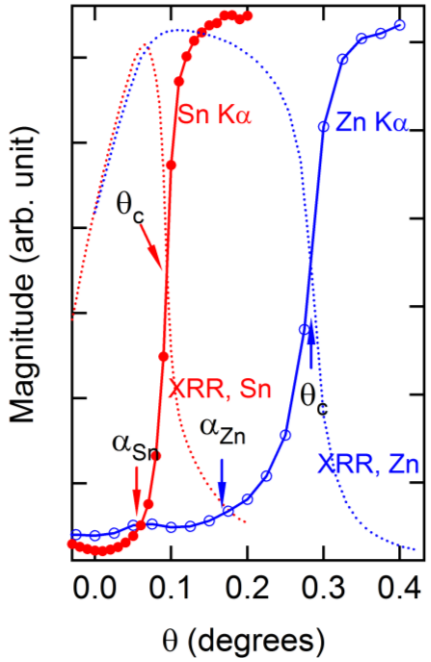

Figure 1. X-ray reflectivity (XRR) and Zn and Sn Kα fluorescence intensities. EXAFS are collected at α_{Sn} and α_{Zn}.

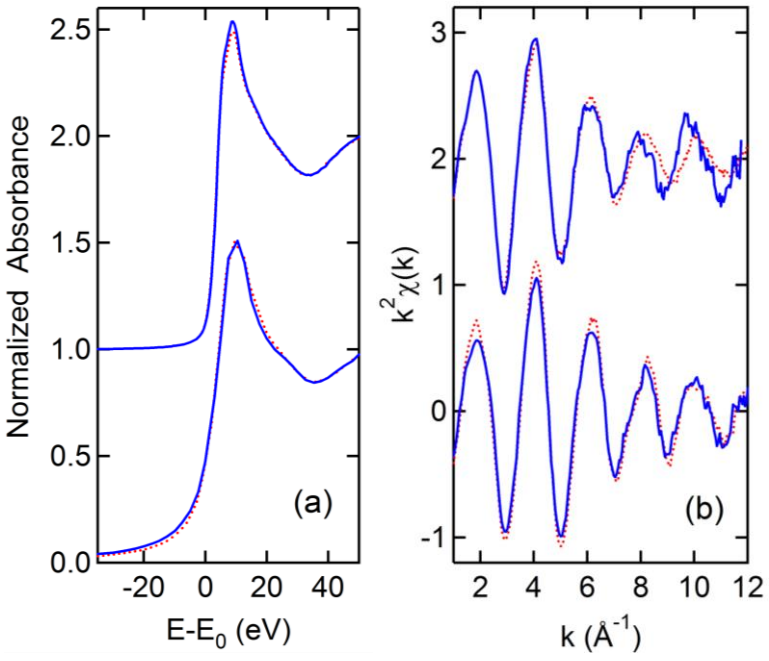

Figure 2. The Zn K edge (upper) and the Sn K edge (lower) X-ray absorption measurements of the *a*-ZTO film: dot lines – film and full lines – surface; (a) XANES; (b) EXAFS.

3. Results and discussion

In a grazing incidence geometry, the EXAFS may be measured through collecting specular reflected intensities, i.e., so called ReflEXAFS, or fluorescence intensities, as the X-ray energy is scanned around an absorption edge E_0 of the element of interest [7]. Yet, the strong correlation between the real δ(E) and imaginary β(E) increments of the refraction index n ($= 1 - \delta - i\beta$) makes it cumbersome to extract the structures from the data. Fortunately, under $\alpha < \theta_c$ conditions, the measured signals from both channels contain the same fine structure oscillations proportional to the absorption coefficients [8], and X-ray probing depth reduces to a few nanometers, providing a means to access the top surface of a film.

To avoid the self-absorption effect, the α-dependence of the EXAFS was monitored. It was found to be absent when $\alpha \leq \frac{2}{3}\theta_c$. Figure 2 compares (a) the X-ray absorption near edge structures (XANES) and

(b) the EXAFS, of the film (dots) and film surface (full lines) of the *a*-ZTO film. The surface EXAFS were measured at $\alpha = 0.16^\circ$ ($< \theta_c = 0.28^\circ$) and $\alpha = 0.06^\circ$ ($< \theta_c = 0.1^\circ$) for the Zn K_α and Sn K_α, respectively. Four and ten scans were merged to obtain the data presented in figure 2, respectively. Note that the self-absorption effect is largely absent in the surface data. In fact, the whiteline of the Zn K edge surface data is higher than that of the film, which may indicate a larger coordination number (N).

As seen in figure 2, the surface EXAFS are similar to the film ones up to k~8 $Å^{-1}$, beyond which differences in phases are seen. The Zn-K edge EXAFS is much more so. The origin of differences is unclear, except that they are reproducible experimentally and not an artifact of data processing. Given $\alpha << \theta_c$, these differences are unlikely due to a δ(E) effect. The Fourier transforms (FT) including data > 8.3 $Å^{-1}$ produce a prominent shoulder or satellite peak at a location smaller than the first main peak. This is rather peculiar in that it occurs to the backscattering amplitude of a light element, i.e., oxygen.

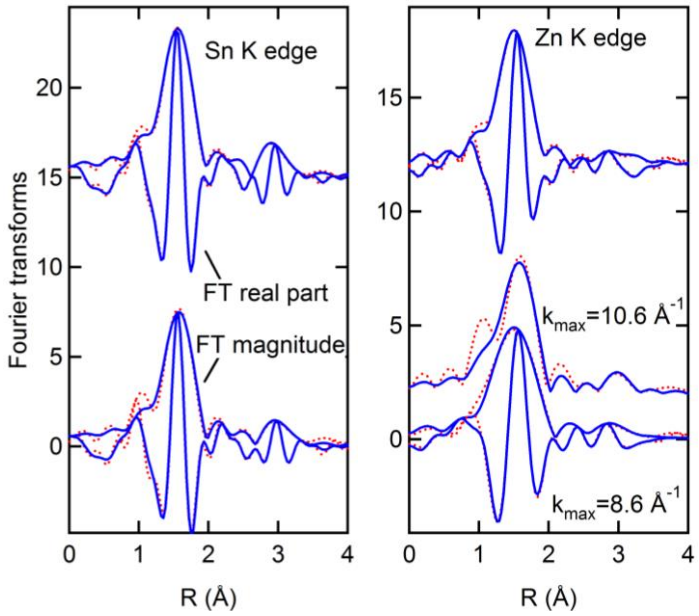

Figure 3. The best fits of Sn K edge and Zn K edge EXAFS spectra of *a*-$Zn_{0.3}Sn_{0.7}O_2$ film (upper) and film surface (lower). Dotted lines: experimental data and full line: curving fittings. For Sn K edge, the result with k = 3.4-11.9 $Å^{-1}$ and R = 1.0-3.6 Å is shown. For Zn K edge: the result with k = 2.3-10.6 $Å^{-1}$ and R = 1.0-3.6 Å is shown for the film EXAFS, and the results with two k ranges are shown (R=1.0-3.6 Å) for the surface EXAFS. Table 1 shows the numerical results. In total, 9 variables are fitted and the independent points ($= 2\Delta r \Delta k/\pi$) are 11 and 14 for k_{max} = 8.6 and 10.6 $Å^{-1}$ for the Zn K edge, respectively, and 14 for the Sn K edge.

The data were quantified by the FEFF8 analyses based on rutile (*r*-) SnO_2 structure using the Artemis software [9]. The amplitude reduction factors S_0^2 were determined to be 0.9 and 1.0 from the EXAFS's of wutzite (*w*-) ZnO and *r*-SnO_2, respectively. For the Zn-O bond, the distance R = 1.96 Å and the bond disorder $\sigma^2 = 4.3\times10^{-3}$ $Å^2$, and 2.06 Å and 3.0×10^{-3} $Å^2$ for the Sn-O bond. Figure 3 shows the best fits. Clearly, the satellite features are not accounted for. This is more apparent for the Zn K edge. The results using two different k ranges are presented to show this effect. Throughout the analyses, the results are weakly dependent on the k_{max} value for the film. This is due to the fact that the oxygen backscattering amplitude is located mainly in the low k region. However, the results of the film surface did show a somewhat larger k_{max} dependence due to the satellite features, whose effect is included in the error bars. Table 1 summarizes the local structures around Zn and Sn. The structures can be well interpreted with single scattering paths of Zn-O, Sn-O and Zn-Sn. Attempts to use Zn-Zn or mix of Zn-Zn and Zn-Sn paths in the fitting yielded no physically meaningful results, indicating no measurable phase separation in the film. For a better fit, it appears that the third cumulant term C_3 in the EXAFS cumulant expansion is needed [10] to account for none Gaussian bonding distribution in this amorphous film.

As seen in Table 1 the local structure around Sn is similar to that of *r*-SnO_2 in which N_1/N_2 = 6/2 and R_1/R_2 = 2.06/3.19 Å, despite high Zn doping level. The structure around Zn is defective. The oxygen vacancies around Zn do not contribute to carrier concentration and are believed to form the neutral vacancies [11]. The short Zn-O bond and the large σ^2 around Zn in the film is a strong indication of how the local structure around Zn is geometrically frustrated which induces strain in the film. E.g., $\sigma^2 = 0.023$ $Å^2$ for the Zn-Sn interaction is equivalent to a spread of the Zn-Sn interaction of ±0.15 Å over its mean.

Therefore, it may not be surprising that this is no longer the case at the surface where the number of this interaction has decreased, resulting a smaller σ^2 for the Zn-Sn interaction at a shorter distance (see Table 1). For a disordered structure whose σ^2 ($= \sigma_S^2 + \sigma_T^2$) is dominated by σ_S^2, such as the one present in this film, the observed N-σ^2 correlation may be largely inherent. Near the surface Zn is fully coordinated (N = 4) likely through oxygen uptake from ambient. Unlike Zn, Sn may have a slightly lower N near the surface and the changes in its local structure are much subdued.

Table 1. Local structures of the film surface and the film (bracketed)

Bonding	*N*	*R* (Å)[§]	$\sigma^2\times10^3$	$C_3\times10^4$
Zn → O	3.9±0.3 (3.4±0.1)	1.99±0.02 (2.01±0.01)	8.9 (6.8)	0.0 (5.4)
Zn → Sn	1.0±0.1 (2.0±0.2)	3.18±0.03 (3.24±0.01)	11.0 (23.0)	30.5 (25.0)
Sn → O	5.7±0.4 (6.0±0.1)	2.06±0.02 (2.06±0.01)	6.2 (5.8)	3.1 (6.4)
Sn → Sn	2.6±0.2 (2.5±0.1)	3.27±0.03 (3.30±0.01)	12.0 (9.9)	2.2 (8.4)

[§]Energy shifts ΔE= 3.6 eV - 6 eV.

3. Summary

We report a surface structure study of an amorphous Zn-Sn-O transparent conducting film using the grazing incidence X-ray absorption technique. By setting the measuring angles far below the critical angle, the details of the surface structure of a film or bulk can be successfully accessed. The measurements show that when $\alpha \leq \frac{2}{3}\theta_c$ the self-absorption effect disappear for systems such as ZnO and SnO_2, which makes this technique suitable for the surface studies of films or bulk. The results show that unlike in the film where Zn is severely under coordinated (N < 4), it is fully coordinated (N=4) near the surface while the coordination number around Sn is slightly less near the surface than in the film. Despite the high Zn doping (30 at. %), the local structure in the film is rutile-like, while some deviation from it is seen around Zn near the film surface. Analyses to link these structural results with the film's physical properties are underway.

ACKNOWLEDGMENT

Film growth and electrical characterization were supported by the NSF funded Materials Research Science and Engineering Center (MRSEC) at Northwestern under Grant No. DMR-1121262. Optical characterization and structural analysis was supported by the ANSER Center, an Energy Frontier Research Center funded by the U.S. Department of Energy, Office of Basic Energy Sciences, under Award No. DE-SC0001059. X-ray absorption and scattering measurements were conducted at the DND-CAT at the Advanced Photon Source (APS). DND-CAT is supported by the NU Office of Research, E.I. DuPont de Nemours & Co., and The Dow Chemical Company. Use of the APS was supported by the U. S. Department of Energy, Office of Science, Office of Basic Energy Sciences, under Contract No. DEAC02-06CH11357.

[1] Ginley D S, Hosono H and Paine D C, in *Handbook of Transparent Conductors*, edited by David S. Ginley (Springer, New York, 2010).
[2] Hoel C A, Mason T O, Gaillard J F and Poeppelmeier K R 2010 *Chem. Mater*. **22** (12) 3569
[3] Kamiya T and Hosono H 2010 *NPG Asia Materials* **2** (1) 15.
[4] Hara H, Hanada T, Shiro T and T Yatabe 2004 *J. Vac. Sci. & Tech. A* **22** (4) 1726.
[5] Ko J H, Kim I H, Kim D, Lee K S, Lee T S, Jeong J H, Cheong B, Baik Y J and Kim W M 2006 *Thin Solid Films* 494 (1-2) 42.
[6] Buchholz D B, Ma Q, Alducin D, Ponce A, Jose-Yacaman M, Khanal R, Medvedeva J E and Chang R P H 2014 *Chem. Mater*. 26 5401
[7] Heald S M, Chen H and Tranquada J M 1988 *Phys. Rev.* B38 1016.
[8] Martens G and Rabe P 1980 *Phys. Stat. Sol*. (a) 58 415.
[9] *http://bruceravel.github.io/demeter/*
[10] Rehr J J and Albers R C 2000 *Rev. Mod. Phys.* 72(3) 621.
[11] Zhu Q, Ma Q, Buchholz D B, Chang R P H, Bedzyk M J and Mason T O 2014 *J Appl. Phys*. 115 033512.